PERGAMON

Automatica 36 (2000) 931–941

www.elsevier.com/locate/automatica

The precise control of manipulators with high joint-friction using base force/torque sensing☆

Guillaume Morel[1], Karl Iagnemma, Steven Dubowsky*

Massachusetts Institute of Technology, Department of Mechanical Engineering, Cambridge, MA 02139, USA

Received 11 May 1998; revised 30 August 1999; received in final form 13 October 1999

Feedback from a base-mounted force/torque sensor can be used to estimate joint torque in robotic manipulators. High precision position control is attainable.

Abstract

Joint friction is a major problem in accurate robot position control, particularly during low-speed, small-amplitude tasks. This paper proposes a simple, practical, and effective method to compensate for joint friction, using a six-axis force/torque sensor mounted under the manipulator. From these measurements, joint torques are estimated and used in a torque controller, which virtually eliminates friction and gravity effects, providing high-precision motion control even for small motions at low speed. The method does not require complex analytical friction models. The method also does not require expensive and unreliable internal joint-torque sensors. Experimental results demonstrate the effectiveness and practicality of the method for an electrical PUMA and hydraulic Schilling Titan II manipulator. © 2000 Elsevier Science Ltd. All rights reserved.

Keywords: Manipulation; Position control; Torque control; Friction

1. Introduction

Precise position and force control is required for many important applications, including the assembly of precision-component systems, micro-manipulation, and robotic surgery (Ku & Salcudean, 1996). These applications often require very small motions at low speeds. Under such conditions, the degrading effects of joint, actuator and transmission friction can dominate system behavior, making precise position and endpoint force control of robotic manipulators difficult to achieve.

The problem is compounded when the manipulator must move heavy objects at slow speeds with high precision. The important problem of nozzle dam placement in nuclear power plant maintenance is such an application (Zezza, 1985). In this application, an hydraulic or highly geared electrical manipulator is required to precisely place a large, heavy nozzle dam. In hydraulic manipulators, joint seal friction is often very high, and likewise in highly geared electrical manipulators, transmission friction is often high. Hence, obtaining precise motion and force control in these systems is very difficult.

Substantial research has been devoted to improving friction-degraded manipulator performance. Direct-drive electrical robots have been proposed and developed that have relatively low joint friction (Asada & Youcef-Toumi, 1987). However, these systems are not appropriate for applications that require the applications of large forces. Also, direct-drive actuators are heavy compared with geared actuators, and thus are not appropriate for applications that require lightweight manipulators, such as space applications (Schenker et al., 1997).

Control methods have also been proposed to reduce the effects of joint friction. Some methods incorporate a mathematical model of friction (Canudas de Wit, 1988). An estimate of frictional forces provided by the model is used either in feedforward or feedback compensation (Armstrong, 1991; Popovic, Shimoga & Goldenberg, 1994). These methods require a precise model. Unfortunately,

☆The original version of this paper was presented at the 5th IFAC Symposium on Robot Control SYROCO '97, Nantes, France, 3–5 September 1997. This paper was recommended for publication in revised form by Associate Editor Y. Nakamura under the direction of Editor K. Furuta.

[1] Present address: The University of Strasbourg, 1-ENSPS, Laboratoires des Sciences de l'Image, de l'Informatique et de la Télédetection, CNRS Strasbourg, France.

* Corresponding author. Tel.: 001-617-253-2144; fax: 001-617-258-7881.
E-mail address: dubowsky@mit.edu (S. Dubowsky).

PII: S0005-1098(00)00007-8

friction is a highly complex, nonlinear phenomena that can depend upon numerous factors, including joint position, load, temperature, and wear (Armstrong, 1991). These factors can be challenging to estimate or measure, and thus model-based friction compensation remains difficult to implement in practical applications.

To overcome modeling difficulties, adaptive methods have been proposed (Canudas de Wit, Olsson, Astrom & Lischinsky, 1996). Dither has also been utilized to improve low-speed positioning performance (Ipri & Asada, 1995). A method that utilizes short-duration torque pulses computed from fuzzy-logic reasoning has also been studied (Popovic, Gorinvesky & Goldenberg, 1995). This approach can be effective in applications where only the final end-effector position is critical. The method cannot control the trajectory that a manipulator takes to reach this final position.

Finally, measurement-based friction compensation methods have been studied (Luh, Fisher & Paul, 1983; Pfeffer, Khatib & Hake, 1989; Vischer & Khatib, 1995). In these methods, the torque applied to a manipulator's links is measured and used as the feedback signal in a torque control loop. Friction is an output disturbance to this control system. With sufficient gain and bandwidth, the torque controller can reject frictional effects. These measurement-based methods have the advantage of being model-free, and have been shown to be effective in practice (Pfeffer et al., 1989; Vischer & Khatib, 1995). However, this approach requires torque sensors mounted at the joint transmission outputs. The use of "indirect sensing" at the actuator level (such as motor current measurements or differential pressure in hydraulic systems) is not appropriate for friction compensation, because the friction disturbance is not measured by these methods. Joint-torque sensors have the drawback of added cost, increased joint flexibility, and additional cabling and electronics. Their complexity can reduce system reliability. Finally, internal sensors must be included during the design of a manipulator, as it is difficult to add them to the existing systems.

In this paper, a new measurement-based joint friction compensation method is presented. The method, called base sensor control (BSC), uses a six-axis force/torque sensor placed under the base of the manipulator (Morel & Dubowsky, 1996; Iagnemma, 1997; Iagnemma, Morel & Dubowsky, 1997). From the measured forces and torques it is possible to calculate the net dynamic torque applied to the links of the manipulator. This measurement is uncorrupted by joint friction. These calculated torques are used in joint-torque controllers. This method eliminates the need for internal joint sensors with the practical problems described above.

The BSC method in its most general form requires dynamic and gravitational models of the system, but no friction model. Nonetheless, the dynamic and gravitational model calculations can be a burden. It is shown that a nearly model-free form of the method can be applied successfully in applications that require low-speed, small-amplitude motions. Experimental results are presented for low-speed, small-amplitude tasks that show that the reduced (i.e. model-free) method can achieve very fine performance. The reduced method requires only simple kinematic coordinate transformations to implement, and hence is easy to apply and does not require substantial computational resources. Results are presented for BSC control of a highly geared PUMA electric manipulator and a hydraulically powered Schilling Titan II manipulator. For both systems, low-speed small-motion performance is greatly improved, even while transporting heavy payloads.

2. Theoretical basis of BSC control

In this section, the equations for joint-torque estimation using a base force/torque sensor are developed.

2.1. General principles

Consider a serial manipulator mounted on a base force/torque sensor as shown in Fig. 1. Classical torque control requires measurement of the dynamic torque applied at each joint i, τ_{d_i}. The total wrench acting at joint, $\mathbf{w}_{t_i}$, can be expressed as the sum of two wrenches:

$$\mathbf{w}_{t_i} = \mathbf{w}_{d_i} + \mathbf{w}_{g_i}, \tag{1}$$

where $\mathbf{w}_{g_i}$ is the wrench due to gravity and $\mathbf{w}_{d_i}$ is the dynamic wrench due to manipulator motion. The 6×1 wrench vector $\mathbf{w}_{d_i}$ is composed of two 3×1 vectors, the force vector $\mathbf{f}_{d_i}$ and the moment vector $\mathbf{m}_{d_i}^{A}$ at an arbitrary point A.

The dynamic torque at joint i, τ_{d_i}, is a component of the wrench $\mathbf{w}_{d_i}$ parallel to the joint i axis, representing the dynamic interaction between links $i-1$ and i:

$$\boldsymbol{\tau}_{d_i} = \mathbf{z}_{i-1}^{T} \mathbf{m}_{d_i}^{O_{i-1}}, \tag{2}$$

where the point O_{i-1} and the unit vector $\mathbf{z}_{i-1}$ define the joint i axis (see Fig. 1). Note that in the following analysis, only rotary joints are considered. However, the method is not restricted to rotary-joint manipulators. For a linear joint, the joint force f_{d_i} along the joint translation axis $\mathbf{z}_{i-1}$ would be given by

$$f_{d_i} = \mathbf{z}_{i-1}^{T} \mathbf{f}_{d_i}. \tag{3}$$

To compute $\boldsymbol{\tau}_{d_i}$ from Eq. (2), or f_{d_i} from Eq. (3), the wrench $\mathbf{w}_{d_i}$ must be derived from the total wrench measured at the base of the robot, $\mathbf{w}_{t_0}$. Note that the base sensor measures the wrench corresponding only to the net forces and torques effectively transmitted to the manipulator's links. Thus, joint and transmission friction do not appear in the measured base wrench, since friction is an internal force.

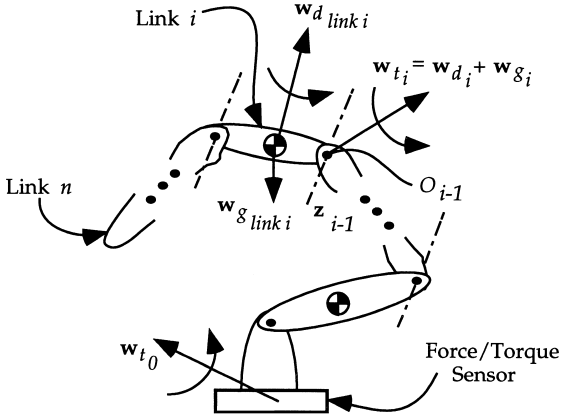

Fig. 1. Serial manipulator mounted on a base force/torque sensor.

The wrench $\mathbf{w}_{d_i}$ can be rewritten from Eq. (1) as

$$\mathbf{w}_{d_i} = \mathbf{w}_{t_i} - \mathbf{w}_{g_i}. \tag{4}$$

The first term on the right-hand side of Eq. (4), $\mathbf{w}_{t_i}$, can be computed from the base wrench by writing the Newton–Euler equations of successive bodies from the base link 0 to link $i-1$:

$$\begin{aligned}
\mathbf{w}_{t_1} &= \mathbf{w}_{t_0} - \mathbf{w}_{d_{\text{link }0}} \mathbf{w}_{g_{\text{link }0}},\\
\mathbf{w}_{t_2} &= \mathbf{w}_{t_1} - \mathbf{w}_{d_{\text{link }1}} \mathbf{w}_{g_{\text{link }1}},\\
&\vdots\\
\mathbf{w}_{t_i} &= \mathbf{w}_{t_{i-1}} - \mathbf{w}_{d_{\text{link }i-1}} - \mathbf{w}_{g_{\text{link }i-1}}.
\end{aligned} \tag{5}$$

Summing equation set (5) leads to

$$\mathbf{w}_{t_1} = \mathbf{w}_{t_0} - \sum_{k=0}^{i-1} \mathbf{w}_{d_{\text{link }k}} - \sum_{k=0}^{i-1} \mathbf{w}_{g_{\text{link }k}}, \tag{6}$$

where $\mathbf{w}_{d_{\text{link }k}}$ is the dynamic wrench due to the motion of link k, and $\mathbf{w}_{g_{\text{link }k}}$ is the gravity wrench due to the mass of link k (see Fig. 1).

The second term on the right-hand side of Eq. (4), $\mathbf{w}_{g_i}$, corresponds to the gravity wrench at joint i. It is the summation of the link gravitational effects for all the links located between joint i and of the manipulator tip (link n, see Fig. 1). Thus

$$\mathbf{w}_{g_i} = \sum_{k=i}^{n} \mathbf{w}_{g_{\text{link }k}}. \tag{7}$$

Combining Eqs. (4), (6) and (7) yields

$$\begin{aligned}
\mathbf{w}_{d_i} &= \mathbf{w}_{t_0} - \left(\sum_{k=0}^{i-1} \mathbf{w}_{g_{\text{link }k}} + \sum_{k=i}^{n} \mathbf{w}_{g_{\text{link }k}} \right) - \sum_{k=0}^{i-1} \mathbf{w}_{d_{\text{link }k}}\\
&= \mathbf{w}_{t_0} - \mathbf{w}_{g_0} - \sum_{k=0}^{i-1} \mathbf{w}_{d_{\text{link }k}} = \mathbf{w}_{d_0} - \sum_{k=0}^{i-1} \mathbf{w}_{d_{\text{link }k}}.
\end{aligned} \tag{8}$$

Eq. (8) shows that in order to compute the dynamic wrench at joint i, $\mathbf{w}_{d_i}$, from the measured base wrench, $\mathbf{w}_{t_0}$, it is necessary to compensate for the total manipulator gravity wrench, $\mathbf{w}_{g_0}$, and the dynamic effects of links located between the base link and link $i-1$. Eq. (2) yields

$$\boldsymbol{\tau}_{d_i} = \mathbf{z}_{i-1}^{\mathrm{T}} \mathbf{m}_{d_0}^{O_{i-1}} - \sum_{k=0}^{i-1} \mathbf{z}_{i-1}^{\mathrm{T}} \mathbf{m}_{d_{\text{link }k}}^{O_{i-1}}. \tag{9}$$

The dynamic torque applied to the links of the manipulator can be computed from the above relationships. Fig. 2 is a flowchart of the joint-torque estimation procedure.

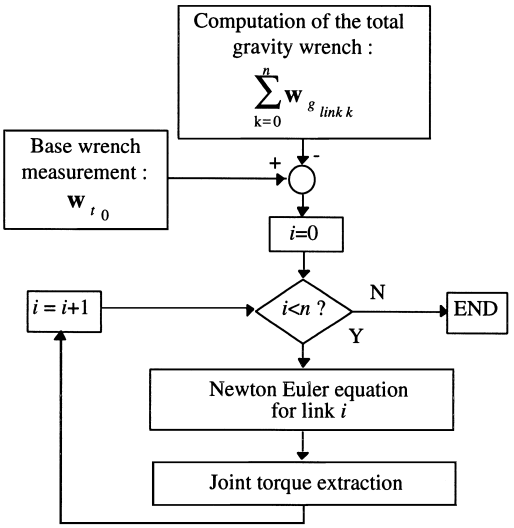

Fig. 2. BSC control algorithm.

2.2. Estimation algorithm

In order to implement the algorithm, it is necessary to develop the expressions of the wrenches $\mathbf{w}_{g_{\text{link }k}}$ and $\mathbf{w}_{d_{\text{link }k}}$ as a function of the manipulator's joint configuration and motion. They can both be expressed at the center of mass G_k of link k:

$$\begin{aligned}
\mathbf{w}_{d_{\text{link }k}} &= \begin{bmatrix} \mathbf{f}_{d_{\text{link }k}} \\ \mathbf{m}_{d_{\text{link }k}}^{G_k} \end{bmatrix} = \begin{bmatrix} m_k \dot{\mathbf{v}}_k^{G_k} \\ \mathbf{I}_k \dot{\boldsymbol{\omega}}_k + \boldsymbol{\omega}_k \times (\mathbf{I}_k \boldsymbol{\omega}_k) \end{bmatrix},\\
\mathbf{w}_{g_{\text{link }k}} &= \begin{bmatrix} \mathbf{f}_{g_{\text{link }k}} \\ \mathbf{m}_{g_{\text{link }k}}^{G_k} \end{bmatrix} = \begin{bmatrix} m_k \mathbf{g} \\ 0 \end{bmatrix},
\end{aligned} \tag{10}$$

where m_k is the mass of link k, $\dot{\mathbf{v}}_k^{G_k}$ is the linear acceleration of link k at G_k, $\mathbf{I}_k$ is the inertia tensor of link k, $\boldsymbol{\omega}_k$ and $\dot{\boldsymbol{\omega}}_k$ are the angular velocities and accelerations, respectively, of link k, and $\mathbf{g}$ is the acceleration due to gravity. Note that all velocities and accelerations are expressed relative to the base frame $\mathbf{R}_0$.

The total gravity moment at the center of the base sensor, point O_0, can then be expressed as the product of a geometry matrix $\mathbf{G}(\mathbf{q})$ and a vector $\mathbf{p}$ of grouped mass

parameters (West, Papadopoulos, Dubowsky & Chean, 1989):

$$\mathbf{w}_{g_0} = \begin{bmatrix} \sum_{k=0}^{n} \mathbf{f}_{g_k} \\ \sum_{k=0}^{n} \mathbf{m}_{g_k}^{O_0} \end{bmatrix} = \begin{bmatrix} \sum_{k=0}^{n} m_k \mathbf{g} \\ \sum_{k=0}^{n} \mathbf{d}_{O_0 G_k} \times m_k \mathbf{g} \end{bmatrix} = \begin{bmatrix} m_{\text{total}} \mathbf{g} \\ \mathbf{G}(\mathbf{q})\mathbf{p} \end{bmatrix}, \quad (11)$$

where m_{total} is the total manipulator mass and $\mathbf{d}_{O_0 G_k}$ is a displacement vector from point O_0 to point G_k. Note that all displacement vectors are expressed in the base frame $\mathbf{R}_0$. Thus, the dynamic wrench at the base can be computed by

$$\mathbf{w}_{d_0} = \mathbf{w}_{t_0} - \mathbf{w}_{g_0} = \begin{bmatrix} \mathbf{f}_{t_0} - m_{\text{total}} \mathbf{g} \\ \mathbf{m}_{t_0} - \mathbf{G}(\mathbf{q})\mathbf{p} \end{bmatrix}. \quad (12)$$

The final torque is then obtained by expanding the terms of Eq. (9). The first term of Eq. (9) can be written as

$$\begin{aligned} \mathbf{z}_{i-1}^{\mathrm{T}} \mathbf{m}_{d_0}^{O_{i-1}} &= \mathbf{z}_{i-1}^{\mathrm{T}} [\mathbf{m}_{d_0}^{O_0} + \mathbf{d}_{O_{i-1} O_0} \times \mathbf{f}_{d_0}] \\ &= [\mathbf{z}_{i-1}^{\mathrm{T}} \mathbf{S}_{O_{i-1} O_0} \quad \mathbf{z}_{i-1}^{\mathrm{T}}] \begin{bmatrix} \mathbf{f}_{d_0} \\ \mathbf{m}_{d_0}^{O_0} \end{bmatrix}, \end{aligned} \quad (13)$$

where $\mathbf{S}_{O_{i-1} O_0}$ is the skew symmetric matrix such that for any vector $\boldsymbol{\alpha}$, $\mathbf{S}_{O_{i-1} O_0} \boldsymbol{\alpha} = \mathbf{d}_{O_{i-1} O_0} \times \boldsymbol{\alpha}$. Since $\mathbf{z}_{i-1}$ and $\mathbf{S}_{O_{i-1} O_0}$ depend only on joint configuration, Eq. (13), combined with Eq. (12), can be written as

$$\mathbf{z}_{i-1}^{\mathrm{T}} \mathbf{m}_{d_0}^{O_0} = \mathbf{A}_i(\mathbf{q}) \begin{bmatrix} \mathbf{f}_{t_0} - m_{\text{total}} \mathbf{g} \\ \mathbf{m}_{t_0}^{O_0} - \mathbf{G}(\mathbf{q})\mathbf{p} \end{bmatrix}, \quad (14)$$

where $\mathbf{A}_i(\mathbf{q}) = \lfloor \mathbf{z}_{i-1}^{\mathrm{T}} \mathbf{S}_{O_{i-1} O_0} \quad \mathbf{z}_{i-1}^{\mathrm{T}} \rfloor$ is a 1×6 vector depending on robot kinematic parameters only.

The second term of Eq. (9) represents a compensation for the effect of the motion of the links between the base and the joint being considered, and can be written as

$$\begin{aligned} \sum_{k=0}^{i-1} \mathbf{z}_{i-1}^{\mathrm{T}} \mathbf{m}_{d_{\text{link } k}}^{O_{i-1}} &= \sum_{k=0}^{i-1} \mathbf{z}_{i-1}^{\mathrm{T}} [\mathbf{m}_{d_{\text{link } k}}^{G_k} + \mathbf{d}_{O_{i-1} G_k} \times \mathbf{f}_{d_{\text{link } k}}] \\ &= \mathbf{z}_{i-1}^{\mathrm{T}} \sum_{k=0}^{i-1} [\mathbf{I}_k \dot{\boldsymbol{\omega}}_k + \boldsymbol{\omega}_k \times (\mathbf{I}_k \boldsymbol{\omega}_k) \\ &\quad + m_k \mathbf{S}_{O_{i-1} G_k} \dot{\mathbf{v}}_k^{G_k}]. \end{aligned} \quad (15)$$

The kth link inertial wrench is a function of link velocity and acceleration. The link velocity $(\mathbf{v}_k^{G_k}, \boldsymbol{\omega}_k)$ is related to joint velocity, $\dot{\mathbf{q}}$, by

$$\begin{aligned} \mathbf{v}_k^{G_k} &= \mathbf{J}_k^{\mathrm{L}}(\mathbf{q})\dot{\mathbf{q}}, \\ \boldsymbol{\omega}_k &= \mathbf{J}_k^{\mathrm{R}}(\mathbf{q})\dot{\mathbf{q}}, \end{aligned} \quad (16)$$

where $\mathbf{J}_k^{\mathrm{L}}(\mathbf{q})$ and $\mathbf{J}_k^{\mathrm{R}}(\mathbf{q})$ are the $3 \times n$ partial Jacobian matrices for linear and rotational motions, respectively. Note that $\mathbf{J}_k^{\mathrm{L}}(\mathbf{q})$ and $\mathbf{J}_k^{\mathrm{R}}(\mathbf{q})$ depend only on the first k link positions. Thus, the $(n-k)$ last columns are zero. Differentiating Eq. (16) with respect to time yields

$$\begin{aligned} \dot{\mathbf{v}}_k^{G_k} &= \mathbf{J}_k^{\mathrm{L}}(\mathbf{q})\ddot{\mathbf{q}} + \dot{\mathbf{J}}_k^{\mathrm{L}}(\mathbf{q}, \dot{\mathbf{q}})\dot{\mathbf{q}}, \\ \dot{\boldsymbol{\omega}}_k &= \mathbf{J}_k^{\mathrm{R}}(\mathbf{q})\ddot{\mathbf{q}} + \dot{\mathbf{J}}_k^{\mathrm{R}}(\mathbf{q}, \dot{\mathbf{q}})\dot{\mathbf{q}}, \end{aligned} \quad (17)$$

where $\ddot{\mathbf{q}}$ is the joint acceleration vector. Combining Eqs. (15)–(17) yields

$$\sum_{k=0}^{i-1} \mathbf{z}_{i-1}^{\mathrm{T}} \mathbf{m}_{d_{\text{link } k}}^{O_{i-1}} = \mathbf{B}_i(\mathbf{q})\ddot{\mathbf{q}} + \mathbf{C}_i(\mathbf{q}, \dot{\mathbf{q}})\dot{\mathbf{q}}, \quad (18)$$

where $\mathbf{B}_i(\mathbf{q})\ddot{\mathbf{q}}$ represents the inertial effects of the first $i-1$ links on the base, projected onto the ith joint axis. The $1 \times n$ column matrix $\mathbf{B}_i(\mathbf{q})$ is given by

$$\mathbf{B}_i(\mathbf{q}) = \mathbf{z}_{i-1}^{\mathrm{T}} \sum_{k=0}^{i-1} [m_k \mathbf{S}_{O_{i-1} G_k} \mathbf{J}_k^{\mathrm{L}}(\mathbf{q}) + \mathbf{I}_k \mathbf{J}_k^{\mathrm{R}}(\mathbf{q})]. \quad (19)$$

The term $\mathbf{C}_i(\mathbf{q}, \dot{\mathbf{q}})\dot{\mathbf{q}}$ represents the centrifugal and Coriolis effects of the first $i-1$ links on the base, projected on the ith joint axis. The $1 \times n$ vector $\mathbf{C}_i(\mathbf{q}, \dot{\mathbf{q}})$ is given by

$$\begin{aligned} \mathbf{C}_i(\mathbf{q}, \dot{\mathbf{q}}) = \mathbf{z}_{i-1}^{\mathrm{T}} \sum_{k=0}^{i-1} [m_k \mathbf{S}_{O_{i-1} G_k} \dot{\mathbf{J}}_k^{\mathrm{L}}(\mathbf{q}, \dot{\mathbf{q}}) + \mathbf{I}_k \dot{\mathbf{J}}_k^{\mathrm{R}}(\mathbf{q}, \dot{\mathbf{q}}) \\ + \mathbf{S}_{\mathbf{J}_k^{\mathrm{R}}(\mathbf{q})\dot{\mathbf{q}}} \mathbf{I}_k \mathbf{J}_k^{\mathrm{R}}(\mathbf{q})]. \end{aligned} \quad (20)$$

Combining Eqs. (9), (14) and (18), and grouping the line vectors $\mathbf{A}_i(\mathbf{q}), \mathbf{B}_i(\mathbf{q})$ and $\mathbf{C}_i(\mathbf{q}, \dot{\mathbf{q}})$ into $n \times n$ matrices, the torque estimation equation becomes

$$\boldsymbol{\tau}_{\mathrm{d}} = \mathbf{A}(\mathbf{q}) \begin{bmatrix} \mathbf{f}_{t_0} - m_{\text{total}} \mathbf{g} \\ \mathbf{m}_{t_0}^{O_0} - \mathbf{G}(\mathbf{q})\mathbf{p} \end{bmatrix} - \mathbf{B}(\mathbf{q})\ddot{\mathbf{q}} - \mathbf{C}(\mathbf{q}, \dot{\mathbf{q}})\dot{\mathbf{q}}, \quad (21)$$

where $\boldsymbol{\tau}_{\mathrm{d}}$ is an $n \times 1$ vector.

Thus, estimation of the torque at each joint requires knowledge of the measured wrench at the base, the manipulator mass properties, and the position, velocity, and acceleration of each joint.

2.3. Simplifying assumptions for fine motion tasks

The implementation of Eq. (21) is, in theory, possible for general tasks. However, it presents some practical problems. First, it requires knowledge of the mass parameters of the manipulator. These parameters are often not well known for industrial systems (An, 1988; Liu, Iagnemma, Dubowsky & Morel, 1998; Raucent, Campion, Bastin, Samin & Willems, 1992). Second Eq. (21) requires measurement or estimation of joint accelerations. The direct measurement of acceleration is difficult to achieve, and computation of acceleration from joint velocity at slow speed can be difficult due to noise corruption. Fortunately, the slow speeds and small motions typical of high-precision tasks allows the dynamic terms in Eq. (21) to be neglected, or

$$\mathbf{B}(\mathbf{q})\ddot{\mathbf{q}} \approx 0, \qquad \mathbf{C}(\mathbf{q}, \dot{\mathbf{q}})\dot{\mathbf{q}} \approx 0. \quad (22)$$

In addition, since precision tasks generally involve small-amplitude motions, the gravitational forces and moments seen at the manipulator base are essentially constant. This constant wrench can be treated as a static offset. All torque estimations can then be based on the difference between the dynamic wrench and the initial static wrench. This static wrench, $\mathbf{w}_{\text{static}}$, is easily obtained by simply reading the base sensor prior to the initiation of the fine-motion task, while the manipulator is stationary.

With these assumptions, Eq. (21) becomes

$$\boldsymbol{\tau}_{\text{d}} = \mathbf{A}(\mathbf{q})[\mathbf{w}_0 - \mathbf{w}_{\text{static}}]. \tag{23}$$

Hence the implementation of the BSC algorithm for precision motion tasks requires only a simple kinematic calculation represented by $\mathbf{A}(\mathbf{q})$. Eq. (23) is a static approximation of the force transmission between the measured wrench and the joint of interest, and $\mathbf{A}(\mathbf{q})$ is the transpose of the manipulator jacobian expressed at O_0. Note that no mass properties of the system need to be identified, and no dynamic model or calculations are required. The method is *nearly* model-free. The experimental results presented below demonstrate the effectiveness of the simplified algorithm.

3. Experimental BSC control of a Puma 550 manipulator

Fig. 3 shows a Puma 550 manipulator mounted on a base force/torque sensor. The manipulator is controlled by a single board 68020 VME computer supporting VxWorks, with a 300 Hz sampling frequency. The base sensor used in these experiments was a modified version of the AMTI OR6-1000 six-axis force/moment sensor (AMTI, 1995). The cost of sensors of this type is approximately 50% greater than the cost of a wrist force/torque sensor with equivalent performance, a small fraction of the cost of adding internal joint torque sensors.

Considering the first three joints of the manipulator, an expression for the matrix $\mathbf{A}(\mathbf{q})$ of Eq. (23) can be written as

$$\mathbf{A}(\mathbf{q}) = \begin{bmatrix} 0 & 0 & 0 & 0 & 0 & 1 \\ 0 & 0 & 0 & s_1 & -c_1 & 0 \\ a_2 s_2 c_1 & a_2 c_2 c_1 & -a_2 c_2 & s_1 & -c_1 & 0 \end{bmatrix}, \tag{24}$$

where a_2 is a Denavit–Hartenberg parameter corresponding to link 2 length ($a_2 = \mathbf{x}_2^{\text{T}} \mathbf{d}_{O_1 O_2}$, see Fig. 3). As discussed above, $\mathbf{B}(\mathbf{q})$ and $\mathbf{C}(\mathbf{q}, \dot{\mathbf{q}})$ are assumed to be zero.

Thus, the torque calculation depends only on the manipulator joint positions, the measured base wrench, and the manipulator's kinematic parameters.

3.1. Friction torque measurements

Experiments were performed to study the nature of the friction in a PUMA 550. The PUMA is a highly geared manipulator, and one would expect to observe substantial joint friction. A voltage was applied to the input of the power amplifiers of the PUMA 550, and the torque at the joints was estimated with the BSC method.

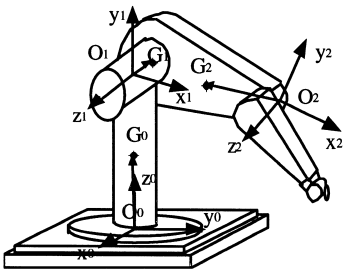

Fig. 3. Puma Denavit–Hartenberg link frames.

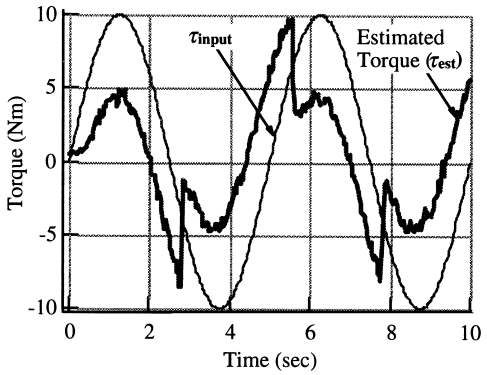

a. Torque Command and Base Sensor Measured Joint Torque

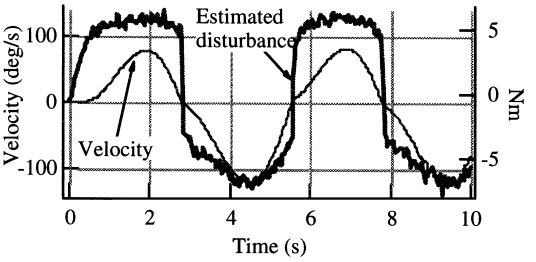

b. Estimated Disturbance Torque and Measured Joint Velocity

Fig. 4. Open-loop experiment for joint 1 of PUMA.

Fig. 4 shows the results for the first joint. The output torque is estimated with Eq. (23). The estimated torque is compared to the commanded motor torque $\boldsymbol{\tau}_{\text{input}}$, which is computed from the motor armature current (i.e. $\boldsymbol{\tau}_{\text{input}}$ is equal to the armature current multiplied by the motor torque constant).

When the system is driven with a sinusoidal input (see Fig. 4a), the output torque measured with the base sensor appears to be the input wave form with a disturbance torque. Fig. 4b shows that the disturbance sign changes when the velocity sign changes, and as expected closely resembles Coulomb friction. Also, note that the

calculated joint torque has very low noise, due to the quality of the force sensor and its electronics.

The magnitude of the Coulomb joint friction shown in Fig. 4b is very large. For the experiment shown, it is approximately equal to 50% of the magnitude of the commanded torque. In fine motion tasks, it would be significantly larger in magnitude than the torque applied to the joint, and performance would be substantially degraded.

3.2. BSC torque control

To compensate for this disturbance, a high-gain integral torque controller with feedforward compensation was considered, of the form

$$\tau_{out} = \tau_{des} + k_{int} \int_0^t (\tau_{des} - \tau_{est}), \tag{25}$$

where τ_{des} and τ_{est} are the desired and the base-sensed torques, respectively (see Fig. 5).

Linear analysis suggests that an integral compensator will provide good performance, achieving low-pass filtering and zero steady-state error (Volpe & Khosla, 1992). A proportional compensator tends to introduce instability, and a derivative compensator is ineffective and difficult to implement. While this analysis also suggests that a feedforward compensator should not be used in conjunction with integral control, the experimental work presented below (with a real nonlinear system) shows some improvement in the torque control performance when a feedforward term is used.

Fig. 6 demonstrates the application of base-sensed torque control to the first joint of the Puma 550. The control gain k_{int} was tuned to 75% of the value that caused experimental structural oscillations.

Here the desired torque is a triangular wave with an amplitude of 3 N m. Note that the experimentally measured dry friction is more than 5 N m. Without torque feedback, the net torque applied to the link would simply be zero, as the friction would be larger than the motor torque. The link would not move. The torque feedback experimental results show that under BSC control the output torque remains very close to its desired value. The current-controlled motor must produce nearly 8 N m to track the desired torque profile. Fig. 6 shows that when the sign of the torque disturbance changes, the torque error peak remains small ($\pm$ 1 N m, i.e. only 20% of the Coulomb friction) and is quickly eliminated by the controller.

3.3. BSC-based position control

Here it is shown that with high-quality torque control provided by the base sensor feedback, it is easy to obtain

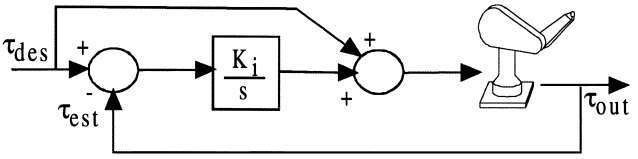

Fig. 5. Torque control block diagram.

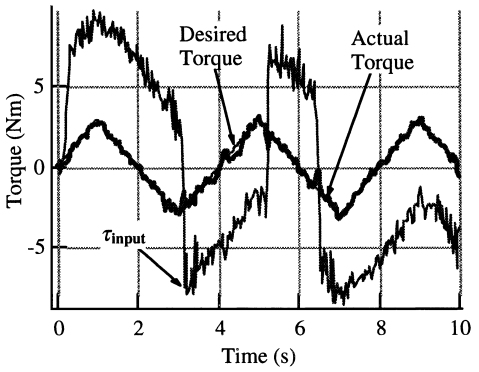

Fig. 6. Joint 1 torque control experimental results.

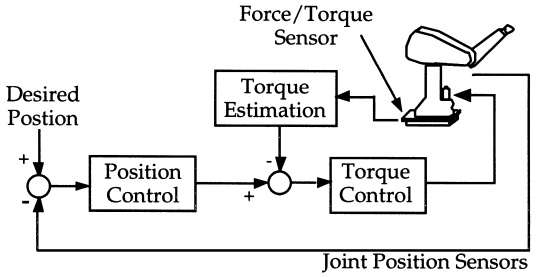

Fig. 7. BSC-based precision position control structure.

precise position control using a simple PD outer loop (see Fig. 7).

Consider the single joint controller given by

$$\tau_{out} = \tau_{des} + k_{int} \int_0^t (\tau_{des} - \tau_{est}) \tag{26}$$

with

$$\tau_{des} = k_p(q_d - q) + k_d(\dot{q}_d - \dot{q}), \tag{27}$$

where k_p and k_d are the proportional and derivative gains, respectively.

Using this controller, joint 1 of the PUMA 550 was commanded to move very slowly, tracking a very low-amplitude triangular wave (see Fig. 8). The magnitude of

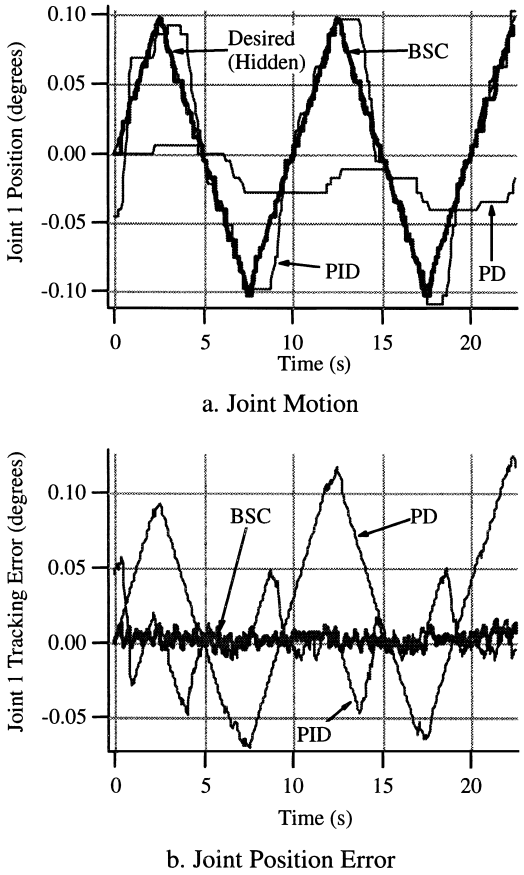

Fig. 8. Comparison of BSC and conventional control for a precise tracking task.

the desired motion is $+/-0.1^{\circ}$, with a period of 10 s. This corresponds to a desired velocity of 7 encoder counts per second. This is a difficult task for a manipulator with high joint friction.

The BSC control method is compared with conventional PD and PID controllers. For these three controllers, the proportional and derivative positions gains have been tuned to provide a bandwidth of 5 Hz and a damping ratio of 0.5. The integral gain in the PID control has been selected to be quite high, equal to 80% of the smallest value exhibiting instability.

Fig. 8 clearly shows improved position control performance provided by the BSC control. Conventional PD control leads to almost no motion, due to coulomb joint friction. The PID controller performs much better, and provides a zero steady-state positioning error. However, when the sign of the velocity changes, the position integral compensator requires a long time (2.5 s) to compensate for the friction, resulting in lack of positioning precision. The base-sensed torque feedback control method compensates rapidly for the Coulomb friction at velocity sign changes (~ 50 ms) and the position error remains close to zero during the entire position profile.

Table 1
Error for 0.1° triangular wave tracking

Controller type	RMS error (deg)	Maximum error (deg)
PID control	0.020	0.056
BSC-based PD control	0.0042	0.012

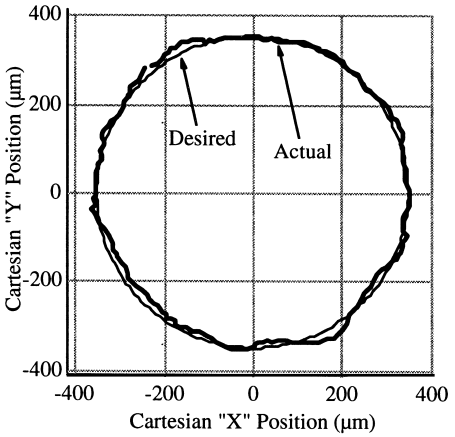

Fig. 9. Cartesian tracking results.

Table 1 summarizes the performance of the three controllers. Conventional (PI) control results in RMS errors 476% greater than BSC control, and the maximum error 466% greater. The results of BSC control show that the resolution of the encoder is reached. An encoder count corresponds to a 0.0058° angle, and thus the root-mean-square error (0.0042°) is less than one encoder count throughout the entire task.

Fig. 9 shows position control results for the PUMA performing a cartesian-space motion task. In this task the end-effector is required to track a circle with a 350 μm radius. The desired trajectory requires the first three joints to perform coordinated motion (the wrist joints are locked during these experiments). The joint-level control scheme is as described above. In the robot configuration selected, the maximum magnitude of the joint motions is 0.1°. The end-effector position was measured using a 2D photodetector and a laser mounted on the robot's end-effector.

Fig. 9 shows the cartesian tracking results in the sensor coordinate frame. It should be noted that, since the motion is cyclic, the sign of the velocity changes at least once in all three joints during the motion. This results in large frictional disturbances. The spite of these perturbations, the precision remains excellent: the maximum absolute position error is less than 30 μm. This is an excellent result considering the substantial joint friction found in the highly geared transmission of this manipulator.

4. Application of BSC control to a hydraulic manipulator

The Schilling Titan II is a six degree-of-freedom industrial hydraulic manipulator (see Fig. 10). It is used widely in undersea and nuclear applications because of its very high strength, low weight, and large workspace. However, it suffers from poor dynamic characteristics, largely due to high joint friction. Performance during small, slow motions is dominated by difficult-to-model nonlinear joint and actuator friction (Armstrong, 1991; Habibi, Richards & Goldenberg, 1994; Lischinsky, Canudas de Wit & Morel, 1999). Base sensor control was implemented in an attempt to improve the low-speed, small-amplitude performance of the Titan II. The control hardware was identical to the PUMA 550 system (see Section 3) with the exception that joint position resolver feedback was converted to encoder-type signals with an effective resolution of 0.087°. The base sensor used in these experiments was a modified version of the AMTI OR6-4000 six-axis force/moment sensor (AMTI, 1995).

The position control scheme had the same form as the system used in PUMA control experiments (see Fig. 7). The inner loop integral compensator provides low-pass filtering, and zero steady-state error. However, while previous theoretical and experimental results for the PUMA showed that an integral compensator with a feedforward term provides the best performance, analysis for the Titan II is less conclusive, due to its highly nonlinear characteristics. It is shown below, however, that an inner loop integral compensator is effective for the Titan II. A simple proportional controller is used for the outer loop. Derivative feedback is not required due to the high damping inherent in the system.

Fig. 11a shows a simple test where the third joint of the Titan II tracks a 1.5° magnitude triangular wave at 0.1 Hz. The commanded trajectory magnitude corresponds to approximately 17 counts of the quadrature-converted resolver signal. Due to the very high joint friction, this motion is difficult to execute.

Proportional and integral gains were tuned to 75% of the level causing structural oscillation. The manipulator under conventional control (shown in Fig. 11a) requires a relatively long time (~ 6 s) to reach zero-error tracking. However, BSC control allows the manipulator to achieve good tracking performance within a much shorter (~ 0.5 s) time. Due to the integral nature of both controllers, tracking performance lags at velocity sign changes (when the frictional force changes direction).

Fig. 11b shows the joint angular errors of the two control approaches, and Table 2 compares the results. Conventional (PI) control results in RMS errors 326% greater than BSC control, and the maximum error 127% greater.

Comparing the performance of the same controllers executing an even smaller amplitude profile (0.5°, 0.1 Hz triangular waveform) also shows the substantial improvement with the base sensor approach (see Table 3). This motion corresponds to a magnitude of approximately 6 counts, and velocity of 2 counts per second.

At these very low speeds, proportional control with base-sensor feedback requires slightly longer to compensate for friction at velocity sign changes (~ 1 s). However, zero steady-state error is still achieved.

Conventional control RMS error is 120% larger than BSC control. While some errors remain for the BSC

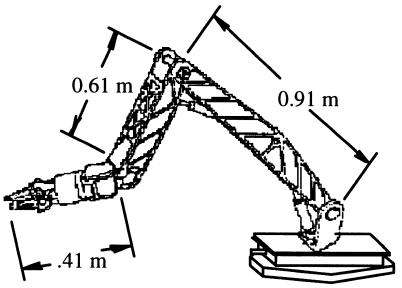

Fig. 10. Schilling Titan II mounted on a force/torque sensor.

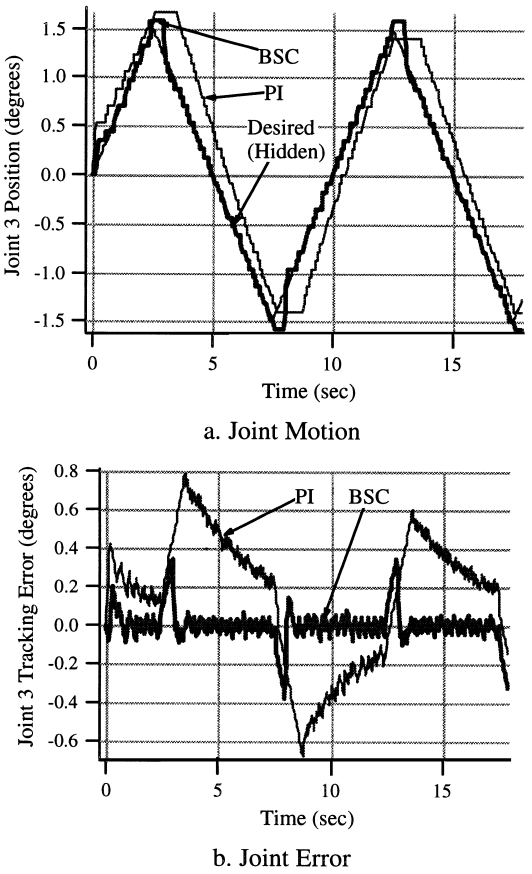

Fig. 11. Joint space tracking comparison for schilling Titan II.

Table 2
Error for 1.5° triangular wave tracking

Controller type	RMS error (deg)	Maximum error (deg)
PI control	0.3671	0.7860
BSC-based P control	0.0861	0.3460

Table 3
Error for 0.5° triangular wave tracking

Controller type	RMS error (deg)	Maximum error (deg)
PI control	0.1863	0.4480
BSC-based P control	0.0845	0.2520

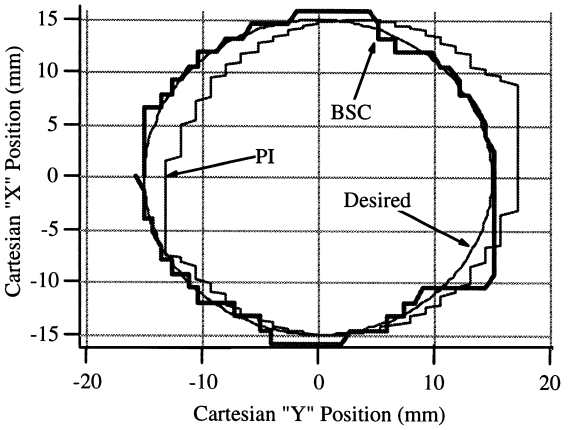

Fig. 12. Cartesian space tracking.

control, recall that this is a very large, powerful manipulator with very high joint friction performing a slow and small motion, a very difficult task.

Cartesian-space experimental results for the Titan II also show substantially improved performance with BSC control. The task shown in Fig. 12 is to track a small circle in cartesian space using joints two and three of the Titan II manipulator. The circle has 15 mm radius and the speed is 0.166 rpm. Recall that the manipulator has a reach of approximately 1.9 m.

This motion requires coupled motion between joints with parallel axes of rotation (joints two and three). This motion will thus test the validity of the torque estimation equation simplifications (i.e. the removal of dynamic terms) since the joint torque information for joints two and three is now highly coupled in the base-sensed wrench.

Table 4
Errors in cartesian-space tracking

Controller type	RMS error (mm)	Maximum error (mm)
PI control	3.033	4.643
BSC-based P control	0.776	1.365

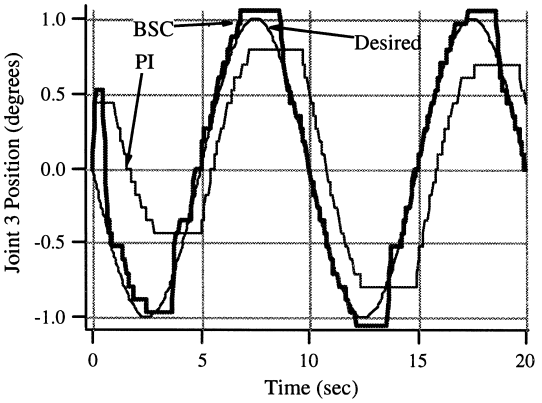

Fig. 13. Tracking comparison with payload.

The effectiveness of the BSC controller for cartesian motion is shown in Fig. 12. Table 4 gives a summary of the results. Clearly, the method results in a significant improvement.

The ability of BSC control to handle large payloads was also investigated. Many industrial tasks require accurate positioning of heavy payloads, such as the placement of the steam generator nozzle dam during nuclear power facility maintenance (Zezza, 1985). A control system must therefore be robust to variations in the effective load on the system, and should provide high-performance control in both loaded and unloaded states. The Titan II is a very lightweight arm (77 kg). An ungeared, lightweight arm which is capable of supporting large loads will be subject to large variations in the effective load on the actuator, a difficult control problem. Here it is shown that the model-free control scheme is robust enough to deal with these variations, and still provide accurate tracking performance.

The commanded task was for the third joint of the Titan II to perform one degree sine wave tracking at 0.1 Hz while supporting a 210 N payload, a substantial load. Fig. 13 compares the tracking performance of PI control and BSC-based P control. From these results it can be seen that with a payload, the performance of PI control is substantially degraded. BSC control performs substantially better. It provides rapid response to friction sign changes, and zero-error tracking is achieved.

5. Conclusions

In this paper a method for compensating for joint friction, using a six-axis force/torque sensor mounted under the manipulator is presented. A simplified form of this method is formulated, which depends only on feedback from the force/torque sensor and manipulator kinematic parameters. The simplified method is shown to greatly improve the positioning performance during fine-motion tasks of a both a highly geared electrical manipulator and an industrial hydraulic manipulator.

Acknowledgements

This work was partially supported by an NSF graduate fellowship, the Korean Electric Power Corporation, and Electricité de France.

References

AMTI (1995). Force/Moment sensor data sheet. Watertown, MA.

An, C. H. (1988). *Model-based control of a robot manipulator*. Cambridge, MA, USA: MIT Press.

Armstrong, B. (1991). *Control of machines with friction*. Boston, USA: Kluwer Academic Publishers.

Asada, H., & Youcef-Toumi, K. (1987). *Direct-drive robots: Theory and practice*. Cambridge, MA, USA: MIT Press.

Canudas de Wit, C. (1988). *Adaptive control of partially known system*. Boston, USA: Elsevier.

Canudas de Wit, C., Olsson, H., Astrom, K. J., & Lischinsky, P. (1996). A new model for control of systems with friction. *IEEE Transactions on Automatic Control*, *40*(3), 419–425.

Habibi, S.R., Richards, R.J., & Goldenberg, A.A. (1994). Hydraulic actuator analysis for industrial robot multivariable control. *Proceedings of the American control conference, 1,* 1003–1007.

Iagnemma, K. (1997). *Manipulator identification and control using a base-mounted force/torque sensor*. S.M. thesis, Department of Mechanical Engineering, Massachusetts Institute of Technology, Cambridge, USA.

Iagnemma, K., Morel, G., & Dubowsky, S. (1997). A model-free fine position control system using the base-sensor: With application to a hydraulic manipulator. *Symposium on robot control, SYROCO '97*, *2*, 359–365.

Ipri, S., & Asada, H. (1995). Tuned dither for friction suppression during force-guided robotic assembly. *IEEE international conference on intelligent robots and systems, 1,* 310–315.

Ku, S., & Salcudean, S. E. (1996). Design and control of a teleoperated microgripper for microsurgery. *Proceedings of the IEEE international conference on robotics and automation*, *1*, 889–894.

Lischinsky, P., Canudas de Wit, C., & Morel, G. (1999). Friction compensation for an industrial hydraulic robot. *IEEE Control Systems Magazine*, *19*(1), 25–32.

Liu, G., Iagnemma, K., Dubowsky, S., & Morel, G. (1998). A base force/torque sensor approach to robot manipulator identification. *Proceedings of the IEEE international conference on robotics and automation, 4*, 3316–3321.

Luh, J., Fisher, W. B., & Paul, R. P. (1983). Torque control by direct feedback for industrial robots. *IEEE Transactions on Automatic Control*, *28*(2), 153–160.

Morel, G., & Dubowsky, S. (1996). The precise control of manipulators with joint friction: A base force/torque sensor method. *Proceedings of the IEEE international conference on robotics and automation, 1*, 360–365.

Pfeffer, L. E., Khatib, O., & Hake, J. (1989). Joint torque sensory feedback of a PUMA manipulator. *IEEE Transactions on Robotics and Automation*, *5*(4), 418–425.

Popovic, M. R., Shimoga, K. B., & Goldenberg, A. A. (1994). Model based compensation of friction in direct drive robotic arms. *Journal of Studies in Information and Control*, *3*(1), 75–88.

Popovic, M.R., Gorinvesky, D.M., & Goldenberg, A.A. (1995). Accurate positioning of devices with nonlinear friction using fuzzy logic pulse controller. *International symposium of experimental robotics, ISER 95* (pp. 206–211).

Raucent, B., Campion, G., Bastin, G., Samin, J. C., & Willems, P. Y. (1992). Identification of the barycentric parameters of robot manipulators from external measurements. *Automatica*, *28*(5), 1011–1016.

Schenker, P.S., Baumgartner, E.T., Lee, S., Aghazarian, H., Garrett, M.S., Lindemann, R.A., Brown, D.K., Bar-Cohen, Y., Lih, S.S., Joffe, B., Kim, S.S., Hoffman, B.H., & Huntsberger, T. (1997). Dextrous robotic sampling for Mars *in-situ* science. *Intelligent robots and computer vision XVI, SPIE Proceedings, 3208*, 170–185.

Vischer, D., & Khatib, O. (1995). Design and development of high-performance torque-controlled joints. *IEEE Transactions on Robotics and Automation*, *11*(4), 537–544.

Volpe, R., & Khosla, P. (1992). An analysis of manipulator force control strategies applied to an experimentally derived model *Proceedings of the IEEE/RSJ international conference on intelligent robots and systems* (pp. 1989–1997).

West, H., Papadopoulos, E., Dubowsky, S., & Chean, H. (1989). A method for estimating the mass properties of a manipulator by measuring the reaction moment at its base. *Proceedings of the IEEE international conference on robotics and automation* (pp. 1510–1516).

Zezza, L. J. (1985). Steam generator nozzle dam system. *Transactions of the American Nuclear Society*, *50*, 412–413.

Guillaume Morel is an assistant professor at the University Louis Pasteur — Strasbourg I, where he is involved with the CNRS/ULP Laboratoire des Sciences de l'Image, de l'Informatique et de la Télédétection. He completed his Ph.D. at the Laboratoire de Robotique de Paris (University of Paris 6) and spent two years as a postdoctoral researcher at the Massachusetts Institute of Technology. His research interests include position and force control of robots, and visual servoing.

Karl Iagnemma received his B.S. in Mechanical Engineering *summa cum laude* from the University of Michigan in 1994, and his M.S. in Mechanical Engineering from the Massachusetts Institute of Technology in 1997, where he was a National Science Foundation Graduate Research Fellow. He is currently completing his Ph.D. in Mechanical Engineering at M.I.T. His research interests include mobile robot planning and control, mobile manipulation, and manipulator identification.

Steven Dubowsky received his Bachelor's degree from Rensselaer Polytechnic Institute of Troy, New York in 1963, and his M.S and Sc.D. degrees from Columbia University in 1964 and 1971. He is currently a Professor of Mechanical Engineering at M. I. T. He has been a Professor of Engineering and Applied Science at the University of California, Los Angeles, a Visiting Professor at Cambridge

University, Cambridge, England, and Visiting Professor at the California Institute of Technology. During the period from 1963 to 1971, he was employed by the Perkin-Elmer Corporation, the General Dynamics Corporation, and the American Electric Power Service Corporation. Dr. Dubowsky's research has included the development of modeling techniques for manipulator flexibility and the development of optimal and self-learning adaptive control procedures for rigid and flexible robotic manipulators. He has authored or coauthored nearly 100 papers in the area of the dynamics, control and design of high performance mechanical and electromechanical systems. Professor Dubowsky is a registered Professional Engineer in the State of California and has served as an advisor to the National Science Foundation, the National Academy of Science/Engineering, the Department of Energy, and the US Army. He has been elected a fellow of the ASME and is a member of Sigma Xi, and Tau Beta Pi.